

## An EUV Study of the Intermediate Polar EX Hydrae

Kunegunda E. Belle<sup>1,2</sup>, Steve B. Howell<sup>1,2</sup>, Martin Sirk<sup>3</sup>, and Mark E. Huber<sup>1,2</sup>

### ABSTRACT

On 2000 May 5, we began a large multi-wavelength campaign to study the intermediate polar, EX Hydrae. The simultaneous observations from six satellites and four telescopes were centered around a one million second observation with *EUVE*. Although EX Hydrae has been studied previously with *EUVE*, our higher signal-to-noise observations present new results and challenge the current IP models. Previously unseen dips in the light curve are reminiscent of the stream dips seen in polar light curves. Also of interest is the temporal extent of the bulge dip; approximately 0.5 in phase, implying that the bulge extends over half of the accretion disk. We propose that the magnetic field in EX Hydrae is strong enough (a few MG) to begin pulling material directly from the outer edge of the disk, thereby forming a large accretion curtain which would produce a very broad bulge dip. This would also result in magnetically controlled accretion streams originating from the outer edge of the disk. We also present a period analysis of the photometric data which shows numerous beat frequencies with strong power and also intermittent and wandering frequencies, an indication that physical conditions within EX Hya changed over the course of the observation. Iron spectral line ratios give a temperature of  $\log T = 6.5 - 6.9$  K for all spin phases and a poorly constrained density of  $n_e = 10^{10} - 10^{11} \text{ cm}^{-3}$  for the emitting plasma. This paper is the first in a series detailing our results from this multi-wavelength observational campaign.

*Subject headings:* accretion — cataclysmic variables — stars: individual (EX Hya) — ultraviolet: stars

---

<sup>1</sup>Astrophysics Group, Planetary Science Institute, 620 N. 6th Ave. Tucson, AZ 85705; keb@psi.edu, howell@psi.edu, mhuber@psi.edu

<sup>2</sup>Dept. of Physics and Astronomy, University of Wyoming, Laramie, WY 82071

<sup>3</sup>Space Sciences Laboratory, University of California, Berkeley, CA 94720; sirk@alma.ssl.berkeley.edu

## 1. INTRODUCTION

Intermediate polars (IPs) have been the focus of numerous studies since they first emerged as a separate class of cataclysmic variables (CVs). Possessing observational characteristics of both dwarf novae and magnetic cataclysmic variables, the current model for intermediate polars paints them as a fusion of these two types of systems. An asynchronously rotating magnetic white dwarf primary accretes magneto-hydrodynamically controlled material from a truncated accretion disk which is fed via an accretion stream by a red dwarf secondary star (Patterson 1994). The magnetically controlled accretion produces observational properties similar to those of a polar, while the visible accretion disk creates its signature double peaked spectral lines and other typical CV properties. The different components of the intermediate polar system: the secondary star, accretion stream, accretion disk, accretion region on the white dwarf surface, and the white dwarf itself, separately dominate in wavelength regions ranging from infrared to X-ray. While this makes IPs very complicated objects to study, it also provides the opportunity to examine a multitude of astrophysical phenomena: from hot plasmas and accretion processes in the presence of high gravity and temperature to stellar astrophysics and binary evolution.

An opportunity for an in-depth observational study of an intermediate polar arose when we were awarded one million seconds of time on the *Extreme Ultraviolet Explorer Satellite (EUVE)* to observe EX Hydrae. In collaboration with other researchers, we used a number of other satellites to obtain simultaneous observations during the *EUVE* observation. X-ray data were obtained with *Chandra* (spectroscopy), the *Rossi X-ray Timing Explorer (RXTE)*, spectroscopy and photometry), and the Unconventional Stellar Aspect (USA) Experiment (photometry). Along with *EUVE*, ultraviolet data were taken with the *Far Ultraviolet Spectroscopic Explorer (FUSE)*, spectroscopy) and the *Hubble Space Telescope (HST)*, spectroscopy). Several ground based observatories were used to obtain optical data: Apache Point Observatory (APO, spectroscopy), Rosemary Hill Observatory (RHO, photometry), and Braeside Observatory (BO, photometry). Infrared spectra were obtained at the United Kingdom Infrared Telescope (UKIRT). This paper is the first in a series which will detail the observations obtained during our campaign.

## 2. REVIEW OF EX HYA IN THE EUV

EX Hya has been the object of many previous observational studies for two main reasons: it is very bright ( $V \sim 13$ ) and, with an inclination of  $i = 77^\circ \pm 1^\circ$  (Hellier et al. 1987; Siegel et al. 1989; Allan et al. 1998), EX Hya is one of only two X-ray eclipsing intermediate polars (the other is XY Ari, Hellier 1997). However, some difficulties arise when interpreting

observational data due to the fact that the relatively long white dwarf spin period of 67.027 minutes is roughly two-thirds that of the relatively short binary orbital period of 98.257 minutes (Kaitchuck et al. 1987). Masses for the white dwarf in EX Hya have been determined using various methods and have yielded a range of values: measurements of the accretion stream shock height and temperature give  $M_{\text{WD}} \sim 0.5M_{\odot}$  (Fujimoto & Ishida 1997; Allan et al. 1998), radial velocities derived from optical time resolved spectra have led to slightly higher values for the white dwarf mass,  $0.78M_{\odot}$  (Hellier et al. 1987), and a mass as high as  $0.85M_{\odot}$  has been calculated using binary star parameters (Hurwitz et al. 1997).

The accretion curtain theory of IPs, developed from high energy studies, suggests that modulation observed on the white dwarf spin period is due to varying optical depths through curtains of accreting material along our line of sight to the emission regions. However, according to recent X-ray observations (Beuermann & Osborne 1988; Singh & Swank 1993; Allan et al. 1998), it is more likely that photoelectric absorption combines with an occultation of one of the accretion poles to give the observed spin modulation. Maximum (minimum) of the spin phase in EX Hya occurs when the upper magnetic pole points away from (toward) the observer.

Prior to this campaign, the most detailed EUV study of EX Hya was that performed by Hurwitz et al. (1997), who obtained 180 ks of data with the *EUVE* satellite. They found the spin phased light curve to be sinusoidal in shape and modulated by a factor of  $\sim 3.7$ , with a maximum count rate of  $\sim 0.30 \text{ s}^{-1}$  occurring at  $\phi \sim 0.05$ . The binary phased light curve exhibits a bulge eclipse which extends over  $\phi \sim 0.6 - 1.0$  (Mauche 1999). This bulge eclipse has a non-zero flux, being  $\sim 0.17$  of the non-bulge eclipsed flux averaged over the white dwarf spin phases, and has an intrinsic column density determined to be  $1.3 \times 10^{20} \text{ cm}^{-2}$  (Hurwitz et al. 1997). There is also a feature attributed to an eclipse by the secondary star at  $\phi = 0.97$  (Mauche 1999) with a centroid which remains constant to within 6 s for all white dwarf phases implying an emission region located within  $\pm 0.5R_{\text{WD}}$  of the white dwarf. The ingress and egress times of the secondary eclipse were used to constrain the EUV emitting region size to be  $< 0.23R_{\text{WD}}$  at 68% confidence (Hurwitz et al. 1997).

The EUV spectra presented in Hurwitz et al. (1997) contain highly ionized iron and neon emission lines which are indicative of a  $10^7$  K plasma and a volume emission measure of  $3 \times 10^{54} \text{ cm}^{-3}$ . Using the volume emission measure and the characteristic cooling time for a  $10^7$  K plasma, they determined the accretion rate onto the white dwarf to be  $\dot{M}_{\text{WD}} \sim 3 \times 10^{16} \text{ g s}^{-1}$ .

### 3. *EUVE* OBSERVATIONS

EX Hya was observed with the *EUVE* deep survey (DS; 67 – 364Å) instrument and short wavelength spectrometer (SW; 70 – 190Å,  $\Delta\lambda \sim 0.5\text{\AA}$ , Bowyer 1995) continuously for six weeks from 2000 May 5 - June 10, totaling approximately one million seconds of on target time given a  $\sim 30\%$  duty cycle. In spite of two safe holds caused by a battery failure and very high He II  $\lambda 304\text{\AA}$  airglow, the data quality is very good. About 10% of the DS photometer data and a bit less of the SW spectrometer data were rejected during periods of high background/airglow since the deadtime corrections became very large (200 – 700%). Typical DS deadtime corrections for the remaining data were around 115% (i.e., the detector was too busy to process new photons 15% of the time). Two types of products were produced: DS light curves and SW spectrometer spectra, and each is discussed below in detail.

#### 3.1. Photometry

Photometry was performed from the DS images using a circular region of radius 13 pixels centered on the source and an annular background region with an inner radius of 50 pixels and outer radius of 100 pixels (1 pixel =  $4''6$ , Sirk et al. 1997). The photon counts were then binned on a time interval of 10 seconds and barycentric corrections were applied to the mid-time of each bin. From this photometric data set, phase folded light curves were created for the binary period, the white dwarf spin period, and for a few combinations of these two periods (see §4.2). Figure 1 shows the *EUVE* photometric data folded on the white dwarf spin ephemeris,  $T = 2437699.8914(5) + 0.046546504(9)\text{E} - 7.9(4) \times 10^{-13}\text{E}^2$  (Hellier & Sproats 1992), while Figure 2 presents the *EUVE* photometric data folded on the binary ephemeris,  $T = 2437699.94179 + 0.068233846(4)\text{E}$  (Hellier & Sproats 1992). The binary ephemeris phase zero is based on optical binary eclipse timings, while spin phase zero is based on optical spin maxima timings. We will denote the spin phase as  $\phi_{67}$  and the binary phase as  $\phi_{98}$ .

The spin phased light curve (Figure 1), with resolution  $\Delta\phi_{67} = 0.01$  or  $\sim 40$  s, can be fit with the sinusoidal function,  $A + B \sin 2\pi(\phi_{67} - \phi_0)$ , where  $A = 0.122 \pm 0.001$  counts  $\text{s}^{-1}$ ,  $B = 0.097 \pm 0.001$  counts  $\text{s}^{-1}$ , and  $\phi_0 = 0.865 \pm 0.001$ . Maximum occurs at  $\phi_{67} = 0.115 \pm 0.001$  and minimum occurs at  $\phi_{67} = 0.615 \pm 0.001$ ; both values differ from the expected values of  $\phi_{67} = 0.0$  (maximum) and  $\phi_{67} = 0.5$  (minimum), and the maximum phase also differs from a previously determined value of  $\phi_{67} = 0.040 \pm 0.002$  (Mauche 1999). The shift in maximum phase is real as the errors quoted for the spin ephemeris and period (Hellier & Sproats 1992) combine to give an expected error of  $\pm 0.03\phi_{67}$  within the light curve; indicating a possible change in accretion geometry. The count rate at spin maximum is  $\sim 7\times$  the spin minimum

count rate; the non-zero minimum count rate value ( $0.035 \text{ counts s}^{-1}$ ) implies that either part of the EUV emitting region is still in view during the minimum phases, or that there is EUV flux within the binary system not confined to a small occulted region.

Two theories have been advanced to explain the spin modulation in intermediate polars: absorption by an accretion curtain (Hellier et al. 1987) and occultation of the EUV emitting region by the white dwarf (Rosen et al. 1991). While both theories often seem to explain the observed phenomena in different IPs, the EUV flux in EX Hya at minimum is less than half that at maximum, suggesting that if one of the poles is occulted, the other may be partially absorbed or the poles may have very different magnetic field strengths (which could manifest as accretion poles with different temperatures.) For reference, we refer to phases  $\phi_{67} = 0.99 - 0.24$  as spin maximum, phases  $\phi_{67} = 0.24 - 0.49$  correspond to spin decline, phases  $\phi_{67} = 0.49 - 0.74$  are spin minimum, and phases  $\phi_{67} = 0.74 - 0.99$  are spin rise, as illustrated in Figure 1.

EUV modulation seen in the binary light curve (Figure 2, with resolution  $\Delta\phi_{98} = 0.005$  or  $\sim 30$  s) is the result of the inclination angle of EX Hya, rather than emission over the binary orbit. The fluctuations and dips seen throughout the light curve are due to eclipses of varying natures; the large broad dip, or bulge dip, centered at  $\phi_{98} \sim 0.85$ , is caused by an increase in optical depth along our line of sight to the EUV emitting region as viewed through the bulge created by the impact of the accretion stream with the outer edge of the accretion disk. The temporal extent of this dip, from  $\phi_{98} = 0.55 - 1.1$ , implies that the bulge physically extends over half of the accretion disk. The dip at  $\phi_{98} = 0.97$  has generally been attributed to an eclipse of the EUV emitting region by the white dwarf, while the dip at  $\phi_{98} = 1.04$  has not been observed before in EUV or other high energy photometry of EX Hya (e.g., Rosen et al. 1991; Hurwitz et al. 1997; Mauche 1999).

### 3.2. Spectroscopy

To extract the *EUVE* SW spectra, a spectral region 13 pixels tall centered on the spectrum, and two background strips each 100 pixels tall were chosen (1 pixel =  $4''4$ , Abbott et al. 1996). The background spectrum was fit with a smooth Legendre polynomial before subtracting. Utilizing this method ensures that no additional Poisson noise is added to the spectrum (Hurwitz et al. 1997). Spectra were created for a variety of binary and white dwarf spin phases. Figure 3 presents spin phased spectra, but see Figure 2 of Belle, Howell, & Sirk (2002b) for binary phased spectra. The EUV spectra presented here are not significantly better in signal-to-noise per spectrum than those presented in Hurwitz et al. (1997), even though our observations were  $5.5\times$  longer. Assuming equal background levels during both

observations, the signal-to-noise ratio in each of our *four* phase bins should be roughly  $2\times$  greater than the signal-to-noise ratio in each of the two phase bins shown in Hurwitz et al. (1997). However, due to higher solar activity during our observations which increased the *EUVE* background level, the gain in signal-to-noise per spectrum is marginal.

The spin maximum spectrum exhibits the greatest flux, both in the continuum and emission lines, while the spin minimum spectrum has a continuum level consistent with zero. The spin decline and spin rise spectra have average flux levels that are roughly equal to each other, in between the flux levels of the spin maximum and spin minimum spectra. Discerning between a continuum level and a forest of low signal-to-noise emission lines is difficult for these spectra, thus we only identify lines as probable that extend above the  $2\sigma$  error level (adopting a  $3\sigma$  criterion for the lines virtually rules out all line detections.) Table 1 gives the observed wavelengths, fluxes, and the log of the temperature at which the emission line has its greatest power ( $T_{\max}$ ) for the  $2\sigma$  lines identified in the four spin phased spectra along with a few other unblended lines which are used for density determinations (see §4.3). Gaussians were fit to the emission lines in order to determine line parameters and the continuum was taken to be zero in each of the four spectra. The error reported for each  $\lambda_{\text{obs}}$  measurement is a  $1\sigma$  error and does not include the rms error of the SW spectrometer,  $0.11\text{\AA}$ . To aid us in the selection of lines, each listed line was also identified in the summed spectrum. The SW spectrometer has a moderate wavelength resolution of  $0.5\text{\AA}$ , causing many of the emission lines to be blended together. For the lines we believe are blended, both lines are listed in Table 1 for the identification at a single wavelength measurement. Emission lines appearing in the EUV spectra of EX Hya are due to highly ionized iron and neon and have formation temperatures of  $10^{5.7} < T_{\max} < 10^{7.1}$  K.

## 4. DISCUSSION

### 4.1. The Binary Phased Light Curve and Understanding the Binary Ephemeris

The exact interpretation of the phenomena present in the EUV binary light curve of EX Hya is dependent upon the accuracy of the binary ephemeris. Previous EUV and high energy binary light curves of EX Hya have shown a dip at  $\phi_{98} = 0.97$  (or  $\phi_{98} = 0.98$ , Mukai et al. 1998) which has been attributed to a stellar eclipse of the EUV emitting region or white dwarf (Rosen et al. 1988; Mauche 1999). However, there is no direct evidence for a stellar nature of this dip, other than the dip occurs *close* to the expected phase of  $\phi_{98} = 0.0$ . With a new dip appearing at  $\phi_{98} = 1.04$ , similar in nature to the  $\phi_{98} = 0.97$  dip, we are lead to question which, if any, dip is stellar in nature, what could be the cause of a non-stellar

dip, and why the dip at  $\phi_{98} = 1.04$  has not been observed before.

The binary phasing,  $T = 2437699.94179 + 0.068233846(4)\text{E}$ , first determined by Mumford (1967) (ephemeris constants were updated by Hellier & Sproats 1992), and still used today, is based on  $U$  and  $B$  optical light photometric eclipse timings. We note that the error reported in the Mumford (1967) phasing propagates to only  $\pm 0.01\phi_{98}$  today. Photometric eclipses seen in optical light in cataclysmic variables with accretion disks are often due to eclipses of the hot spot by the secondary star. The optical eclipse depth in EX Hya was seen to be shallow and variable over time (Hellier et al. 1987) and during outburst becomes broad and shallow (Reinsch & Beuermann 1990) implying that the accretion disk is eclipsed rather than the white dwarf. Thus, photometric phase zero according to the Mumford (1967) binary ephemeris for EX Hya is likely to be a hot spot eclipse and not true binary zero (i.e., inferior conjunction of the secondary star).

How does the binary ephemeris photometric phase zero compare with spectroscopic phase zero and true binary zero? A stellar eclipse of the hot spot (or bulge) denotes photometric phase zero, while spectroscopic phase zero is taken to occur at the red-to-blue crossing of the optical emission line radial velocity curve; the latter theoretically occurring at inferior conjunction of the secondary star. However, due to a bias in the (disk) emission lines from the hot spot, the red-to-blue crossing can occur approximately when the hot spot is moving perpendicular to the observer’s line of sight. For example, Mason et al. (2000) showed that for cataclysmic variables with a strong optical emitting hot spot, a phase offset exists between spectroscopic and photometric phase zero; a stellar eclipse of the hot spot would occur prior to the hot spot being perpendicular to our line of sight. The measured radial velocity curves of the  $H\beta$  and  $H\gamma$  optical emission lines of EX Hya exhibit a red-to-blue crossing which lags photometric binary phase zero by approximately 0.035 in phase (Hellier et al. 1987). The optical emission lines are likely to be biased by the motion of the hot spot (Hellier et al. 1987) so that the red-to-blue crossing may be interpreted as occurring when the hot spot is traveling approximately perpendicular to the observer’s line of sight. Thus, traveling along the binary orbit, true binary phase zero would occur first, followed by photometric phase zero, and then spectroscopic phase zero, i.e., an eclipse of the white dwarf by the secondary star (if present) would be seen before photometric phase zero.

Applied to EX Hya, this implies that an eclipse of the white dwarf by the secondary would be seen at a phase prior to photometric binary zero, such as  $\phi_{98} = 0.97$ . However, the minimum depth of a stellar eclipse is likely to remain constant and not be dependent upon the spin phase during which it is observed. We will show in the following section that a constant minimum is not the case for this “eclipse”. Therefore, although the phasing of the dip at  $\phi_{98} = 0.97$  may be correct for a stellar “eclipse”, its classification as such is still

questionable.

## 4.2. Comparative Light Curves

The identification of the origin of the dips seen at  $\phi_{98} = 0.97$  and  $\phi_{98} = 1.04$  is facilitated by examining the binary phased light curve extracted at different spin phases (Figure 4). An intriguing feature of the EUV light curves is the relative intensity of the dips at phases  $\phi_{98} = 0.97$  and  $\phi_{98} = 1.04$ . Table 2 provides the unscaled mid-dip count rates for both the  $\phi_{98} = 0.97$  and  $\phi_{98} = 1.04$  dips. The  $\phi_{98} = 0.97$  dip is shallowest during the spin maximum phase and not noticeably different from the other small dips appearing throughout these light curves. The count rate at dip minimum in the spin maximum light curve ranges from  $\sim 20\times$  greater than the mid-dip count rate in the spin minimum light curve to  $\sim 2\times$  greater than the mid-dip count rate in the spin decline light curve. The difference between mid-dip count rates for the  $\phi_{98} = 1.04$  dip is not as extreme, with the spin maximum mid-dip count rate being  $\sim 8\times$  greater than the spin minimum mid-dip count rate, ranging to  $\sim 2\times$  greater than the spin decline value.

Gaussians were fit to the  $\phi_{98} = 0.97$  and  $\phi_{98} = 1.04$  dips in the averaged and all four spin phased binary light curves. The results of the Gaussian fits are given in Table 3. The errors on the measured midpoint values fall within the light curve resolution of  $0.005\phi_{98}$ . The midpoint of the  $\phi_{98} = 0.97$  dip appears to be consistent between the spin maximum and spin rise phases, at  $\phi_{98} = 0.969$ , and between the spin minimum and decline phases at  $\phi_{98} = 0.972$ , however, within the resolution of  $0.005\phi_{98}$ , these values are the same. The  $\phi_{98} = 1.04$  dip midpoint is also consistent in phase at  $\phi_{98} = 1.038$ . FWHM and FWZI values are a bit more scattered. The FWHM values for both dips are the same, within errors, between spin maximum and minimum. The spin rise and decline FWHM values are scattered and show no coherent pattern as are the FWZI values for each dip over all spin phases. The short duration of both dips implies that the region being eclipsed is most likely small in size and close to the white dwarf surface, i.e. the inner accretion curtain close to the accretion pole where the EUV radiation is emitted.

Other asymmetries between the binary EUV light curves of EX Hya in Figure 4 are seen within the broad dip extending from  $\phi_{98} \approx 0.55 - 1.1$ , which is attributed to photoelectric absorption of the accretion region by the bulge or hot spot (Cordova et al. 1985). This broad dip feature has been seen in the light curves of previous EUV and X-ray studies of EX Hya (Cordova et al. 1985; Rosen et al. 1988; Hurwitz et al. 1997). Rosen et al. (1988) show a broad dip which extends for approximately  $\phi_{98} \sim 0.7 - 0.97$  in the  $0.02 - 2.5$  keV band and has an asymmetric shape with a gradual decline and rapid rise while the eclipse seen



in Cordova et al. (1985) (0.04 – 2.0 keV) is a little wider in phase. The EUV bulge dip as shown in Hurwitz et al. (1997) and Mauche (1999) extends from  $\phi_{98} \approx 0.65 - 1.02$  and shows the same gradual decline and rapid rise as the binary light curve presented in this paper.

In a typical cataclysmic variable or intermediate polar system with an accretion disk, the hot spot, the region where the mass transfer stream impacts with the accretion disk, is centered around binary phase 0.8 – 0.9 and does not extend “backwards” past the line of centers. Two things make the bulge in EX Hya atypical; it physically extends over half of the outer edge of the accretion disk (see also Hellier et al. 2000 who present a *B*-band light curve of EX Hya with an orbital hump extending from  $\phi_{98} \sim 0.6 - 1.15$ ), and it extends past binary phase zero. However, we do note that some non-magnetic cataclysmic variables also exhibit an extended hot spot region (e.g., Z Cha, Wood et al. 1986).

The bulge dip appears slightly different when compared between each spin phase as shown in Figure 4. Several differences between the bulge dips in the different light curves are immediately obvious: for example, during the maximum phase, the bulge dip is shallower and has a more gradual decline. However, the temporal extent of the bulge dip appears to be the same in all spin phases, with the exception of an extra shallow dip, preceding the bulge dip, from  $\phi_{98} \sim 0.4 - 0.6$  in the spin minimum light curve. One could argue that the reason for the more rapid decline in flux in the spin minimum light curve is simply due to the fact that there is already a higher optical depth along the line of sight (the accretion curtain) to the accretion pole during the minimum phase. However, this absorption effect would act to absorb the emission by the same amount throughout the entire binary orbit rather than causing extra absorption at a particular binary phase. In the early phases of the bulge dip,  $\phi_{98} \sim 0.65 - 0.7$ , the spin maximum count rate is  $\sim 12\times$  greater than the spin minimum count rate. Comparing this value to the count rate difference in the averaged spin light curve ( $\sim 7\times$ , Figure 1), it is obvious that there must be extra absorption in addition to the accretion curtains during the bulge dip phases.

A change in bulge size is likely to manifest itself observationally in wavebands additional to the EUV, and indeed, we do see a difference when comparing our optical data to the optical light curves from previous studies. For example, our *B*-band light curve compared with the *B* light curve of Mumford (1967) shows a decreased eclipse depth and very prevalent optical sidebands (see Figure 7 of Belle et al. 2002b for a comparison of the light curves). Speculating that these sidebands might be seen in the EUV photometry of EX Hya, we phased our EUV photometric data on common optical orbital sidebands (or beat frequencies) usually seen in intermediate polars:  $\omega \pm \Omega$ ,  $\omega \pm 2\Omega$ , and  $2\Omega$ , where  $\omega$  is the spin frequency and  $\Omega$  is the binary orbital frequency. Coherent modulation, to some degree, was seen on all of these beat frequencies.

In order to investigate the modulations seen on the orbital sidebands and other periods, we searched our EUV photometry for periods using the phase dispersion minimization (PDM) routine (Stellingwerf 1978). PDM provides statistical testing for a given period via a two-sided F-test. Figure 5 presents the results of this analysis, in the form of a thetogram, with the y-axis representing  $\Theta$  which expresses frequency significance, with lower values of  $\Theta$  indicating more statistically significant frequencies. The photometric data was searched for periodicity over time intervals of 10 min (144 cycles day<sup>-1</sup>) to 20 days (0.05 cycles day<sup>-1</sup>), consistent with the available sampling window provided by our long data set and the Nyquist sampling limit. For the data set shown in Figure 5, which contains 97,274 samples, a value of  $\Theta = 0.976$  defines the 99% confidence level for period believability. The 95% confidence level is near  $\Theta = 0.99$ . The occurrence of sampling aliases was lowered by increasing the bin size over which the data were searched, as recommended by Stellingwerf (1978).

We see that in Figure 5 essentially all the periods found are real, they are very well defined, and we have identified a few frequencies of interest on the figure, including that for the *EUVE* satellite orbital period ( $P_{\text{sat}} = 93.73$  min).<sup>4</sup> There are approximately 50 frequencies with  $\Theta$  values above the 95% confidence level ( $\Theta = 0.99$ ) appearing in the thetogram. We have identified all of these frequencies as beats between the spin, orbit, and satellite frequencies, but have only labeled the more common beat frequencies on Figure 5, and frequencies that have been identified in previous photometry of EX Hya. The  $\Omega/2 = 7.33$  day<sup>-1</sup> frequency is strong with  $\Theta = 0.92$  and many of the frequencies appearing in the range 0 – 10 day<sup>-1</sup> are satellite beat frequencies, but we have not labeled these frequencies in order to avoid confusion on the plot. The strongest beat frequencies are those between the satellite and orbit or spin frequency, rather than between the orbit and spin frequencies. We note that the orbital frequency,  $\Omega$ , is much stronger in the EUV than in our optical and X-ray data ( $\Omega$  and  $\omega$  have roughly equal strengths in the EUV, while  $\omega$  is  $\sim 2\times$  stronger than  $\Omega$  in the optical, and  $\sim 1.2\times$  stronger in the X-ray), which is the cause of the numerous beat frequencies visible in the Figure 5.

Figure 6 is a time-sampled thetogram, where the gray scale indicates  $\Theta$  as in Figure 5. This plot was made by a modified version of the PDM code allowing for time-sampled thetograms to be produced. Here we used 5000 data points per segment, and then stepped through the entire data set by increments of 500 data points (data point refers to a 10 sec bin and the sets of data points do not necessarily have equal time sampling). We thus produced the trailed thetogram seen in Figure 6, which covers the time period from 2000 May 5 to June 10, the entire *EUVE* observation. Along the y-axis, one time step refers to a bin of 5000

---

<sup>4</sup>The nominal satellite period was 94.78 min, however, during this observation, the period varied between 93.86 and 93.60 minutes. We would like to thank the anonymous referee for calling this to our attention.

data points. The known periods and sidebands, including the satellite beat frequencies, are fairly constant and strong throughout the temporal sampling covered in the plot. However, there are some interesting frequencies around  $25 \text{ day}^{-1}$  and  $33 \text{ day}^{-1}$  which appear suddenly in the middle of the data set. These frequencies are likely to be beat frequencies, but their appearance during only part of the observation is intriguing and suggests that one or more of the beating frequencies is not constant throughout the data set, i.e., the geometry and/or physical conditions of EX Hya are evolving, to some extent. The frequencies appearing at  $\sim 26 \text{ day}^{-1}$  are associated with the frequencies  $\omega/2 + \Omega$  and  $\omega/2 + \Omega_{\text{sat}}$  but it is interesting to note that what appears to be the  $\omega/2 + \Omega$  frequency wanders back and forth throughout the entire data set.

The appearance of the wandering and intermittent periods in our high energy data probably indicates that there are additional or changing sources of reprocessing of the EUV radiation. These may always be present in the EUV or may be manifestations of the variable nature of EX Hya. A detailed study of the periodicities seen in our contemporaneous observations of EX Hya in the X-ray, EUV, UV, and optical will be presented in a future work.

### 4.3. EUVE Spectra

Figure 3 presents EUV spectra extracted from the four white dwarf spin phases, as described in Figure 1, and Table 1 presents the stronger lines we have identified in each spectrum, along with their fluxes and  $\log T_{\text{max}}$ . The emission lines seen in these spectra are from highly ionized neon and iron, with the coolest lines (neon) having  $T_{\text{max}} = 10^{5.7} \text{ K}$  and the hottest lines (iron) having temperatures of  $T_{\text{max}} = 10^{7.1} \text{ K}$ . Only five lines appear (above the  $2\sigma$  error) in each of the four spin phased spectra, four of which are blended: Fe XV  $\lambda 73.47\text{\AA}$ , Fe XX  $\lambda 93.78\text{\AA}$ /Fe XVIII  $\lambda 93.93\text{\AA}$ , and Fe XXIII  $\lambda 132.84\text{\AA}$ /Fe XX  $\lambda 132.85\text{\AA}$ . These lines have  $\log T_{\text{max}} = 6.3, 6.9, 6.7, 7.1,$  and  $6.9 \text{ K}$ , respectively. Using the flux ratios of these lines, we can further confine the temperature range of the emitting plasma. According to the optically thin plasma model of Mewe, Gronenschild, & van den Oord (1985), the flux ratios of the lines at  $\lambda 132/\lambda 93\text{\AA}$ ,  $\lambda 132/\lambda 73\text{\AA}$ , and  $\lambda 93/\lambda 73\text{\AA}$  match those expected for a  $\log T \sim 6.5 - 6.9 \text{ K}$  plasma. The flux ratio determined temperature is in agreement with the  $T_{\text{max}}$  values of the individual lines. However, if we consider the flux ratio of the two Ne lines we have identified in the spin maximum and decline spectra, Ne VIII/Ne VI  $\lambda 98\text{\AA}$  to Ne VIII  $\lambda 88\text{\AA}$ , the plasma temperature determination is significantly lower, near  $\log T \sim 5.8 \text{ K}$ , for both spin phases.

Line ratios may also be used to determine plasma densities according to Mewe et al.

(1985), Table IVa, using lines that have  $\log T_{\max} = 7.0$  K. Only two of the four spectra have emission lines near this temperature which are unblended: spin maximum and spin decline. The *spin maximum* line ratio, Fe XX  $\lambda 110.63\text{\AA}$ /Fe XXII  $\lambda 114.39\text{\AA}$  =  $0.57 \pm 0.22$ , gives a density of  $> 10^{14} \text{ cm}^{-3}$  (note that Fe XX  $\lambda 110.63\text{\AA}$  actually has  $\log T_{\max} = 6.9$ ). The line ratio of Fe XXI  $\lambda 117.51\text{\AA}$ /Fe XXI  $\lambda 121.21\text{\AA}$  =  $0.80 \pm 0.72$  in the *spin decline* spectrum gives a lower density,  $n_e = 10^{10} - 10^{11} \text{ cm}^{-3}$  ( $n_e < 10^{13} \text{ cm}^{-3}$  when considering the lower limit determined from the uncertainty). These values may indicate an observed density range, although poorly constrained. We would like to note that the density determined from the  $\lambda 110/\lambda 114$  line ratio does have a problem, as the ratio uses lines from two different charge states and depends strongly on the plasma temperature. For example, if we were to initially assume a low density plasma, Table IV of Mewe et al. (1985) shows that the value of the  $\lambda 110/\lambda 114$  ratio measured here matches well with a  $\log T_{\max} \sim 6.8$  K. Considering that our spin decline line ratio finds a low density, it is likely that assuming a constant temperature of  $T = 10^7$  K for the  $\lambda 110/\lambda 114$  ratio does not adequately take into account the strong dependence on temperature of the different charge states, and that the lines are likely to be formed in a lower density plasma.

Using only the reliably determined density above ( $n_e = 10^{10} - 10^{11} \text{ cm}^{-3}$ ), our value does not agree with the electron densities which have been previously determined for EX Hya. Hurwitz et al. (1997) found an electron density of  $n_e \geq 10^{13} \text{ cm}^{-3}$  using the ratio of the Fe XX/Fe XXIII blend to the Fe XXI emission lines in their *EUVE* spectra. Mauche, Liedhal, & Fournier (2001) found a value of  $n_e \geq 3 \times 10^{14} \text{ cm}^{-3}$  from our *Chandra* spectrum using the Fe XVII  $\lambda 17.10/\lambda 17.05\text{\AA}$  line ratio. We note that while these two values are self-consistent, the Hurwitz et al. (1997) value was determined from blended lines in different charge states and the Mauche, Liedhal, & Fournier (2001) ratio is affected by photoexcitation.

The appearance of the Fe XXIII/Fe XX lines at  $\lambda 132\text{\AA}$  in each spectrum (except during mid-bulge dip, see Figure 2 of Belle et al. 2002b) suggests that a high temperature plasma ( $10^7$  K) is constantly in view during the times in which we see other EUV emitting regions of lower temperature and lower density. The absence of the  $\lambda 132\text{\AA}$  line, and also the  $\lambda 93\text{\AA}$  line, during the mid-bulge dip phase suggests that these lines are formed interior to the bulge and that their emitting region is roughly confined to the orbital plane.

The emission line centers appear to shift over the four spin phases. Each spin phase is comprised of many orbital phases, so radial velocities of these lines will be a complex sum of both motions. Also, a radial velocity curve over spin phase will not have much meaning when only containing four points. However, it is interesting to note that the Fe XXIII/Fe XX blend at  $\lambda 132\text{\AA}$  has a fairly constant negative velocity at all spin phases with an average value of  $-260 \pm 180 \text{ km s}^{-1}$ . The other two strong lines which appear in each of the four spectra also

have negative velocities over all four spin phases. The Fe XV  $\lambda 73.47\text{\AA}$  emission line has its most blue-shifted velocity of  $-980 \pm 245 \text{ km s}^{-1}$  during spin maximum and its lowest blue-shifted velocity of  $-531 \pm 572 \text{ km s}^{-1}$  during spin decline. The Fe XX/Fe XVIII blend at  $\lambda 93\text{\AA}$  is not blue-shifted to the same extent and has its greatest blue-shift of  $-463 \pm 256 \text{ km s}^{-1}$  during spin minimum. The SW spectrometer rms error of  $0.11\text{\AA}$  (Abbott et al. 1996), which has not been added to the  $1\sigma$  errors given for the line velocities above, translates to a velocity error of  $450 \text{ km s}^{-1}$  at  $73\text{\AA}$ ,  $350 \text{ km s}^{-1}$  at  $93\text{\AA}$ , and  $250 \text{ km s}^{-1}$  at  $132\text{\AA}$ ; even assigning a systematic maximum uncertainty to the line velocities, we note that the emission lines are generally still blue-shifted. (The  $\gamma$ -velocity of EX Hya has not been subtracted from these values due to the fact that it is not well constrained.)

Taken at face value, the phase-independent blue-shifts of the emission lines in the *EUVE* spectra tell us that the lines may be associated with some outflowing material. However, we note that Mauche, Liedhal, & Fournier (2001) reported that the Fe XVII  $\lambda 15 - 17\text{\AA}$  emission lines had a wavelength offset consistent with zero (though the error from the wavelength accuracy they quote does allow these lines to be blue-shifted.) The accretion pole regions would be a likely site for outflowing material in the form of a wind or jet. The disappearance of the  $\lambda 132\text{\AA}$  line during the bulge dip would mean that the poles must be highly inclined with respect to the spin axis if the cause of its blue-shift is due to jets. We believe instead that this outflow may originate as a wind from the inner edge of the accretion disk, a feature common in high mass transfer binaries, possibly associated with shocks in the accretion disk (see below). Such an emission site would constantly provide outflowing material directed at the observer, while also being absorbed during the bulge dip phases. In an upcoming paper discussing our *HST* data (Belle et al. 2002a), we show that blue-shifted absorption components (P Cygni profiles), features which are indicative of outflowing material, are seen in several of the UV emission lines.

## 5. A REVISED MODEL FOR EX HYA

The current intermediate polar model has the white dwarf evenly accreting matter from an annular accretion disk via accretion curtains onto both magnetic poles (e.g., Patterson 1994). However, King & Wynn (1999) have recently shown that EX Hya exists in a spin equilibrium state such that this model may not hold true. They first note that although a disk may form in any intermediate polar, it is generally far from Keplerian due to the influence of the magnetic field on the accretion flow in the disk. For EX Hya, where the spin period is close to the binary orbital period ( $P_{\text{spin}}/P_{\text{orb}} = 0.68$  for EX Hya compared with  $P_{\text{spin}}/P_{\text{orb}} \sim 0.1$  for other IPs), the equilibrium condition is such that the corotation and the

circularization radii are roughly equal to the distance to the inner Lagrange point  $L_1$ . This condition is true for a special class of intermediate polars which possess a white dwarf with a magnetic moment of  $2 \times 10^{33} \text{ G cm}^3 \lesssim \mu_1 \lesssim 10^{34} \text{ G cm}^3$  (and  $P_{\text{orb}} < 2 \text{ hr}$ ), corresponding to a magnetic field strength of 2 – 7 MG for the white dwarf in EX Hya.

The EUV data presented in this paper support the model alluded to by the King & Wynn (1999) study in which non-uniform accretion from the disk onto the white dwarf magnetic poles occurs. The extended bulge dip seen in the binary light curve (Figure 2), the absorption dips seen throughout the binary light curves of Figure 4, along with the differing absorption amounts seen between these same light curves are all evidence of non-uniform accretion. We propose that the magnetic field in EX Hya is strong enough to begin pulling some material vertically from the outer edge of the disk, thereby forming a large accretion curtain which would produce the very broad and extended bulge. Material after binary phase 0 would accumulate as it encounters the bulge in the accretion disk. This concept is depicted in Figure 7 (although we have drawn accretion curtains which extend only from the inner or outer disk, it is more likely that there would be a continuous curtain extending between the two disk edges.) Matter attaching to the magnetic field lines at the outer edge of the disk would form accretion streams which would act to absorb radiation emitted from the accretion poles and would produce dips within the binary light curves, such as those seen at  $\phi_{98} = 0.97$  and  $\phi_{98} = 1.04$ . These dips are reminiscent of dips seen in polar light curves (e.g., Belle, Howell, & Mills 2000). Inspection of Figure 4 shows that the dips at  $\phi_{98} = 0.97$  and  $\phi_{98} = 1.04$  have varying depths (values are given in Table 2), with the dips during spin minimum having the greatest amount of absorption. At spin and binary phases such that spin minimum and the bulge eclipse are coincident ( $\phi_{67} = 0.37 - 0.87$  and  $\phi_{98} = 0.6 - 1.0$ ), material in the bulge, already extending above the plane of the disk, may be controlled by the magnetic field and produce denser streams.

If the dips seen in the binary phased light curve are caused by material attached to the field lines, why are the dips seen along the binary phase rather than the spin phase? The reality of the magnetic field attachment to the outer edge of the disk is that the field lines will be affected by magnetic torque such that the lines will become twisted. While the white dwarf magnetic pole has already started to rotate away from the bulge, the distortion of the magnetic field caused by the torque will allow the field lines to remain attached at the bulge. As long as the field lines remain attached, matter will be kept from falling back down to the accretion disk. In this way, the dips would be seen along the binary phase rather than the spin phase.

If the scenario just described is true for EX Hya, the strength of the magnetic field needed

to pull material from the outer edge of the disk can be estimated. Using the equation,

$$r_\mu = 9.9 \times 10^{10} \mu_{34}^{4/7} M_{\text{WD}}^{-1/7} \dot{M}_{16}^{-2/7} \text{ cm} \quad (1)$$

to calculate the radius of the magnetosphere (Warner 1995) and setting  $r_\mu$  equal to the outer accretion disk radius, we can solve for  $\mu_{34}$ . We use white dwarf masses of  $0.48 M_\odot$  (Fujimoto & Ishida 1997) and  $0.85 M_\odot$  (Hurwitz et al. 1997) to represent the range of primary masses which have been determined for EX Hya. Optical spectroscopic emission line velocities (our optical data will appear in a future paper), and the white dwarf mass range, give the outer disk radius as  $1.6 \times 10^{10}$  or  $4.3 \times 10^{10}$  cm. With an accretion rate of  $1 \times 10^{16} \text{ g s}^{-1}$  (Hurwitz et al. 1997), we find a magnetic field strength of  $\sim 1 - 8$  MG. We would like to note that using the optical emission line velocities to determine the disk radius assumes that some of the disk is in Keplerian motion.

The far-reaching magnetic field has implications other than producing an extended bulge. As stated previously, the circularization radius is roughly equal to the corotation radius (King & Wynn 1999). This intimates that part or possibly all of the accretion disk is rotating with the white dwarf. Although we do not know the latitude of the magnetic poles on the white dwarf surface, the modulation seen on the spin period suggests that the poles are moderately inclined ( $\sim 10^\circ$ , Kim & Beuermann 1995, 1996) with respect to the rotation axis of the white dwarf. The accretion disk, then, would not feel a constant magnetic force, but rather would feel the highest field strength at the regions of the disk closest to the poles. At these locations along the disk, the disk material would be more affected by the magnetic field strength and hence would become controlled by the magnetic field. Thus, we have a situation in which some amount of material in two chunks, or pie slices (one facing each pole), along the accretion disk are rotating with the white dwarf, while the rest of the accretion disk may (or may not) be rotating with the white dwarf. The outer disk velocities measured from the optical spectra are around  $500 - 600 \text{ km s}^{-1}$ , while the velocity of the magnetic field sweeping through the disk is calculated at the corotation radius ( $R_{\text{co}} = 3.5 \times 10^{10} \text{ cm}$ ) to be  $\sim 550 \text{ km s}^{-1}$ , again enforcing the statement that the outer disk is corotating with the white dwarf magnetic field.

An issue pertaining to the corotating pie slices in the accretion disk is the presence of shocks which may form as matter of different velocities interacts in the accretion disk. Modeling shocks is beyond the scope of this paper, however, we argue that the similar velocities of the white dwarf and accretion disk (as discussed previously) would produce very low energy shocks. High energy emission lines are already seen in the spectra and because the bulge dip eclipses all EUV emission (i.e., we cannot distinguish between the white dwarf or accretion disk being eclipsed), it is not possible to discern if these lines originate in a shock from the accretion disk, or from the shocks and high energy plasmas associated with

regions near the magnetic accretion poles. However, if the shocks produce winds, they may be responsible for the highly blue-shifted lines seen in the EUV spectra.

Another question to answer is why strong power is not seen at the  $\omega - \Omega$  frequency if the magnetic field is coupled to the accretion disk (though we note that while this frequency is not strong, it is above the 95% confidence level.) This might be expected if there was a bright EUV point source situated on the edge of the disk, however, the outer edge of the disk is vertically extended and cool and will emit most strongly at lower energies, such as optical wavelengths. We will show in a future paper describing our optical data that strong power *is seen* on the  $\omega - \Omega$  frequency. We should also consider the possibility that an overflow accretion stream may be responsible for the small dips seen at  $\phi_{98} = 0.97$  and  $\phi_{98} = 1.04$ , instead of magnetically controlled streams causing these dips. We argue that this is not likely for several reasons. First, there are many dips seen throughout the bulge dip, starting at  $\phi_{98} \sim 0.6$  and continuing through to  $\phi_{98} \sim 0$ , which makes it likely that these dips are caused by material associated with the bulge. Second, the overflow stream is unlikely to extend far enough above the orbital plane in order to be along the line of sight to the accretion poles. Third, this overflow stream would follow along its ballistic trajectory and would not be in a position to cause a dip occurring after binary phase 0.

## 6. CONCLUSION

The photometric and spectroscopic data presented here have provided us with some intriguing results for EX Hya. This system clearly does not conform to the traditional intermediate polar model. A broad bulge dip, numerous smaller dips throughout the binary light curve, and the inconsistencies between binary light curves extracted at different spin phases all indicate that EX Hya may be accreting material from the outer edge of the accretion disk thereby producing an extended bulge and large accretion curtain. For material at the outer edge of the disk to become magnetically controlled, the magnetic field of the white dwarf must be on the order of 1 – 8 MG. These extended regions may also be reprocessing sites of EUV radiation, as can be seen from the many strong beat frequencies appearing in the single thetagram (Figure 5) and time-series thetagram (Figure 6). Iron spectral line ratios give a temperature of  $10^{6.5} - 10^{6.9}$  K for the emitting plasma but provide only a poorly constrained density of  $n_e = 10^{10} - 10^{11} \text{ cm}^{-3}$ . It is likely that regions of varying temperature and density are viewed simultaneously throughout the spin orbit. Future papers will investigate the physical meaning of the strong frequencies in greater detail, along with relating the EUV data to our other wavelength observations.



We would like to thank C. Mauche for his contributions and comments on this work and the anonymous referee for very valuable comments. This research was partially supported by NASA grant NAG5-8644 to SBH.

## REFERENCES

- Abbott, M. J. et al. 1996, *ApJS*, 107, 451
- Allan, A., Hellier, C., & Beardmore, A. 1998, *MNRAS*, 295, 167
- Belle, K. E., et al. 2002a, in preparation
- Belle, K. E., Howell, S. B., & Mills, A. 2000, *PASP*, 112, 343
- Belle, K. E., Howell, S. B., & Sirk, M. 2002b, in *ASP Conf. Ser. 264, Continuing the Challenge of EUV Astronomy: Current Analysis and Prospects for the Future*, ed. S. Howell, J. Dupuis, D. Golombek, F. Walter, & J. Cullison (San Francisco: ASP), 96
- Beuermann, K. & Osborne, J. P. 1988, *A&A*, 189, 128
- Bowyer, S. 1995, *Proc. SPIE*, 2517, 97
- Córdova, F. A., Mason, K. O., & Kahn, S. M. 1985, *MNRAS*, 212, 447
- Fujimoto, R. & Ishida, M. 1997, *ApJ*, 474, 774
- Hellier, C. 1997, *MNRAS*, 291, 71
- Hellier, C., Kemp, J., Naylor, T., Bateson, F. M., Jones, A., Overbeek, D., Stubbings, R., & Mukai, K. 2000, *MNRAS*, 313, 703
- Hellier, C., Mason, K. O., Rosen, S. R., & Córdova, F. A. 1987, *MNRAS*, 228, 463
- Hellier, C. & Sproats, L. N. 1992, *IBVS*, 3724
- Hurwitz, M., Sirk, M., Bowyer, S., & Ko, Y.-K. 1997, *ApJ*, 477, 390
- Kaitchuck, R. H., Hantzios, P. A., Kakaletis, P., Honeycutt, R. K., & Schlegel, E. M. 1987, *ApJ*, 317, 765
- King, A. R. & Wynn, G. A. 1999, *MNRAS*, 310, 203
- Kim, Y. & Beuermann, K. 1995, *A&A*, 298, 165

- Kim, Y. & Beuermann, K. 1996, *A&A*, 307, 824
- Mason, E. et al. 2000, *MNRAS*, 318, 440
- Mauche, C. W. 1999, *ApJ*, 520, 822
- Mauche, C. W., Liedhal, D. A., & Fournier, K. B. 2001, *ApJ*, 560, 992
- Mewe, R., Gronenschild, E. H. B. M., & van den Oord, G. H. J. 1985, *A&AS*, 62, 197
- Mukai, K., Ishida, M., Osborne, J., Rosen, S., & Stavroyiannopoulos, D. 1998, in *ASP Conf. Ser. 137, Wild Stars in the Old West*, ed. S. Howell, E. Kuulkers, C. Woodward (San Francisco: ASP), 554
- Mumford, G. S. 1967, *ApJS*, 15, 1
- Patterson, J. 1994, *PASP*, 106, 209
- Reinsch, K. & Beuermann, K. 1990, *A&A*, 240, 360
- Rosen, S. R., Mason, K. O., & Córdova, F. A. 1988, *MNRAS*, 231, 549
- Rosen, S. R., Mason, K. O., Mukai, K., & Williams, O. R. 1991, *MNRAS*, 249, 417
- Siegel, N., Reinsch, K., Beuermann, K., van der Woerd, H., & Wolff, E. 1989, *A&A*, 225, 97
- Singh, J. & Swank, J. 1993, *MNRAS*, 262, 1000
- Sirk, M. M., Vallergera, J. V., Finley, D. S., Jelinsky, P., & Malina R. F. 1997, *ApJS*, 110, 347
- Stellingwerf, R. F. 1978, *ApJ*, 224, 953
- Warner, B. 1995, *Cataclysmic Variable Stars* (Cambridge: Cambridge Univ. Press)
- Wood, J., Horne, K., Berriman, G., Wade, R., O’Donoghue, D., & Warner, B. 1986, *MNRAS*, 219, 629

Table 1. Identified bright EUV spectral emission lines.

Ion $\lambda$ ( $\log T_{\max}$ ) ( $\text{\AA}$ ) (K)	Spin Phase							
	Maximum $\lambda_{\text{obs}}^{\text{a}}$ ( $\text{\AA}$ )	Flux <sup>b</sup>	Decline $\lambda_{\text{obs}}$ ( $\text{\AA}$ )	Flux	Minimum $\lambda_{\text{obs}}$ ( $\text{\AA}$ )	Flux	Rise $\lambda_{\text{obs}}$ ( $\text{\AA}$ )	Flux
Fe XV 73.47 (6.3)	$73.23 \pm 0.06$	$11.9 \pm 3.60$	$73.34 \pm 0.14$	$8.04 \pm 5.18$	$73.30 \pm 0.06$	$10.3 \pm 3.44$	$73.27 \pm 0.05$	$12.1 \pm 4.14$
Ne VIII 88.08 (5.8)	$88.03 \pm 0.26$	$3.75 \pm 3.29$	$87.95 \pm 0.08$	$1.97 \pm 0.91$	$88.00 \pm 0.08$	$1.43 \pm 0.60$	...	...
Fe XX 93.78 (6.9)/ Fe XVIII 93.93 (6.7)	$93.83 \pm 0.04$	$5.28 \pm 0.73$	$93.85 \pm 0.06$	$4.94 \pm 0.85$	$93.71 \pm 0.08$	$2.16 \pm 0.62$	$93.78 \pm 0.07$	$3.53 \pm 0.98$
Ne VIII 98.13 (5.8)/ Ne VI 98.20 (5.7)	$98.16 \pm 0.06$	$6.13 \pm 1.08$	$98.33 \pm 0.12$	$3.23 \pm 1.27$	...	...	...	...
Fe XXI 102.21 (7.0)/ Fe XXII 102.23 (7.0)	$102.21 \pm 0.05$	$2.48 \pm 0.76$	...	...	...	...	$102.20 \pm 0.10$	$2.71 \pm 1.05$
Fe XX 110.63 (6.9)	$110.62 \pm 0.06$	$2.16 \pm 0.67$	...	...	...	...	$110.77 \pm 0.10$	$2.41 \pm 0.96$
Fe XXI 113.30 (7.0)/ Fe XX 113.34 (6.9)	$113.26 \pm 0.06$	$3.90 \pm 0.71$	$113.20 \pm 0.09$	$2.17 \pm 0.78$	...	...	...	...
Fe XXII 114.39 (7.0)	$114.28 \pm 0.05$	$3.80 \pm 0.85$	...	...	...	...	...	...
Fe XXII 117.17 (7.0)	$117.07 \pm 0.05$	$3.41 \pm 0.78$	$117.09 \pm 0.07$	$1.87 \pm 0.80$	...	...	...	...
Fe XXI 117.51 (7.0)	...	...	$117.70 \pm 0.04$	$0.99 \pm 0.51$	...	...	...	...
Fe XXI 121.21 (7.0)	...	...	$121.19 \pm 0.10$	$1.24 \pm 0.92$	...	...	...	...
Fe XXIII 132.84 (7.1)/ Fe XX 132.85 (6.9)	$132.74 \pm 0.03$	$9.11 \pm 1.48$	$132.72 \pm 0.04$	$5.01 \pm 1.23$	$132.71 \pm 0.06$	$2.02 \pm 0.95$	$132.74 \pm 0.07$	$4.55 \pm 1.67$

<sup>a</sup>Errors on all  $\lambda_{\text{obs}}$  measurements are  $1\sigma$  errors and do not include the rms error of the SW spectrometer.

<sup>b</sup>Fluxes are in units of  $10^{-4}$  photons  $\text{s}^{-1}$   $\text{cm}^{-2}$ .

Table 2. Binary light curve mid-dip count rates.

Spin Phase	$\phi_{98} = 0.97$ (% max) <sup>a</sup> (counts s <sup>-1</sup> )	$\phi_{98} = 1.04$ (% max) (counts s <sup>-1</sup> )
Maximum	0.070 ± 0.009 (–)	0.089 ± 0.010 (–)
Minimum	0.003 ± 0.004 (5)	0.011 ± 0.005 (13)
Rise	0.018 ± 0.007 (25)	0.035 ± 0.009 (40)
Decline	0.032 ± 0.007 (45)	0.055 ± 0.008 (62)

<sup>a</sup>“% max” indicates the dip count rate as a percentage of the maximum mid-dip count rate.

Table 3. Gaussian fit results for the two strongest photometric dips.

Spin Phase	$\phi_{98} = 0.97$			$\phi_{98} = 1.04$		
	Midpoint <sup>a</sup> ( $\phi_{98}$ )	FWHM ( $\Delta\phi_{98}$ )	FWZI ( $\Delta\phi_{98}$ )	Midpoint ( $\phi_{98}$ )	FWHM ( $\Delta\phi_{98}$ )	FWZI ( $\Delta\phi_{98}$ )
Averaged	0.970	0.010 ± 0.001	0.024	1.037	0.018 ± 0.002	0.044
Maximum	0.969	0.012 ± 0.001	0.019	1.038	0.018 ± 0.002	0.041
Minimum	0.972	0.014 ± 0.001	0.025	1.037	0.018 ± 0.002	0.031
Rise	0.969	0.010 ± 0.001	0.030	1.038	0.022 ± 0.001	0.045
Decline	0.972	0.016 ± 0.001	0.030	1.037	0.012 ± 0.001	0.025

<sup>a</sup>Errors on the midpoint values fall within the resolution of the light curves.

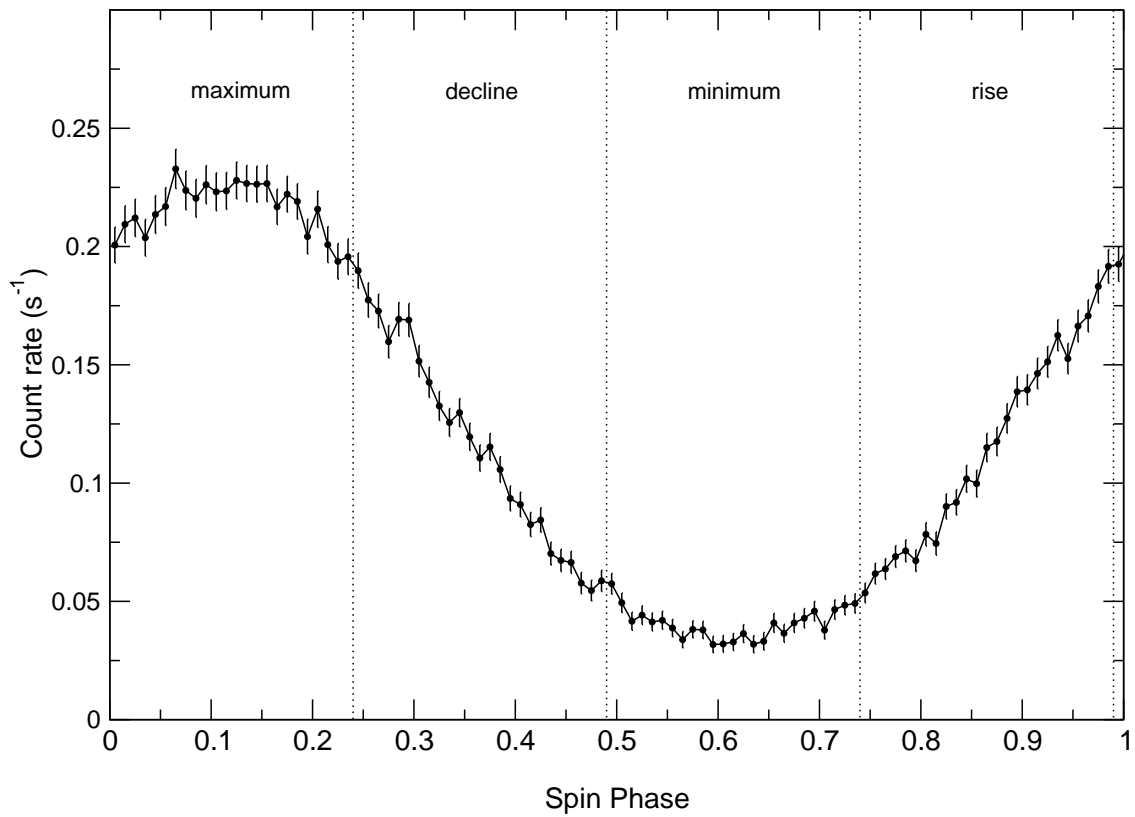


Fig. 1.— Summed EUVE spin phased light curve. This light curve has a resolution of  $\Delta\phi_{67} = 0.01$  or  $\sim 40$  s. Spin phase delimitations are labeled.

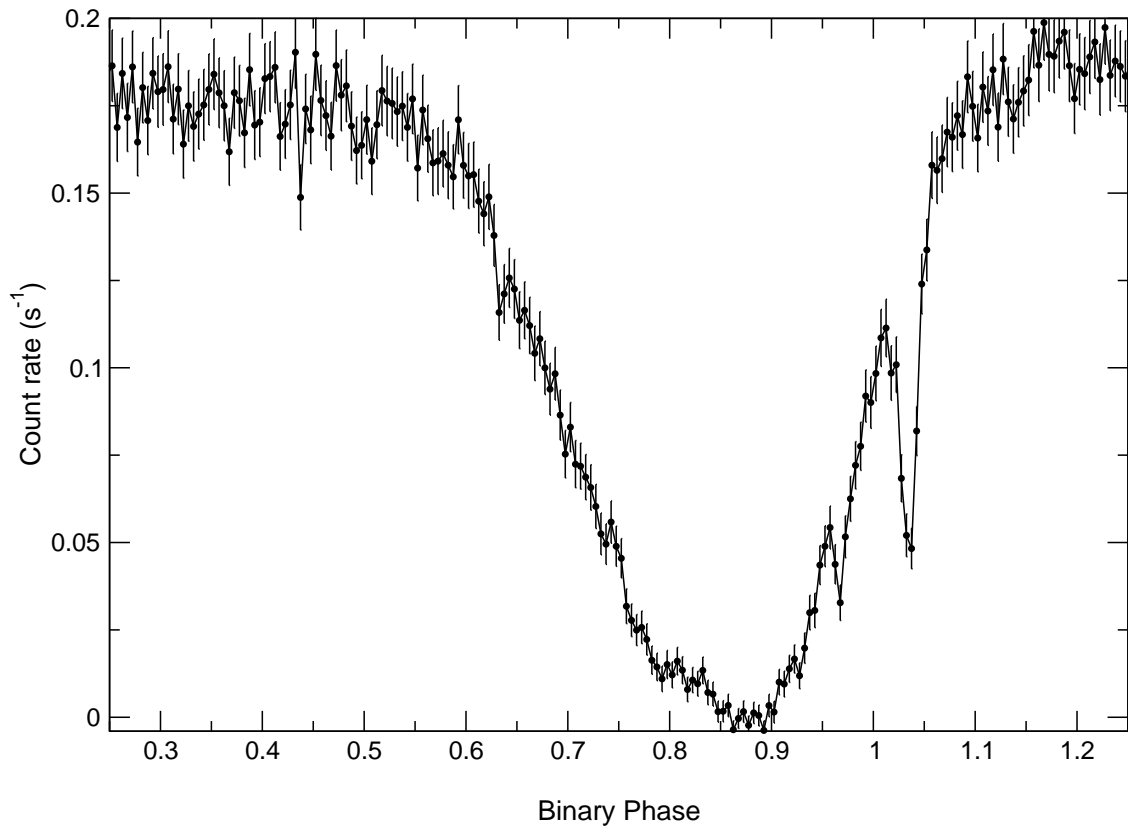


Fig. 2.— Summed binary phased EUVE light curve. The resolution is  $\Delta\phi_{98} = 0.005$  or  $\sim 30$  s.

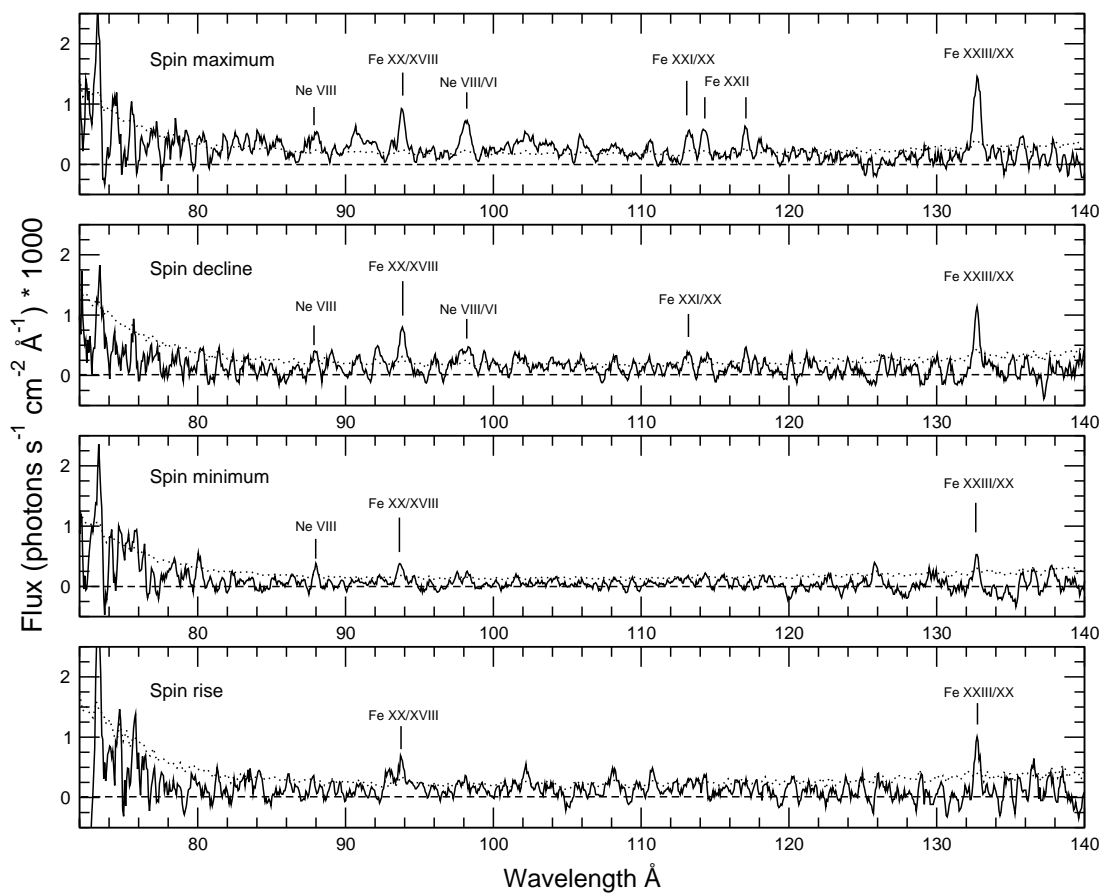


Fig. 3.— *EUVE* SW spectra combined on four spin phases. From top to bottom they are spin maximum, decline, minimum, and rise. Some of the stronger lines from Table 1 have been labeled in this plot. See Table 1 for the complete list of identified lines. The dotted line represents the  $1\sigma$  error for each spectrum.

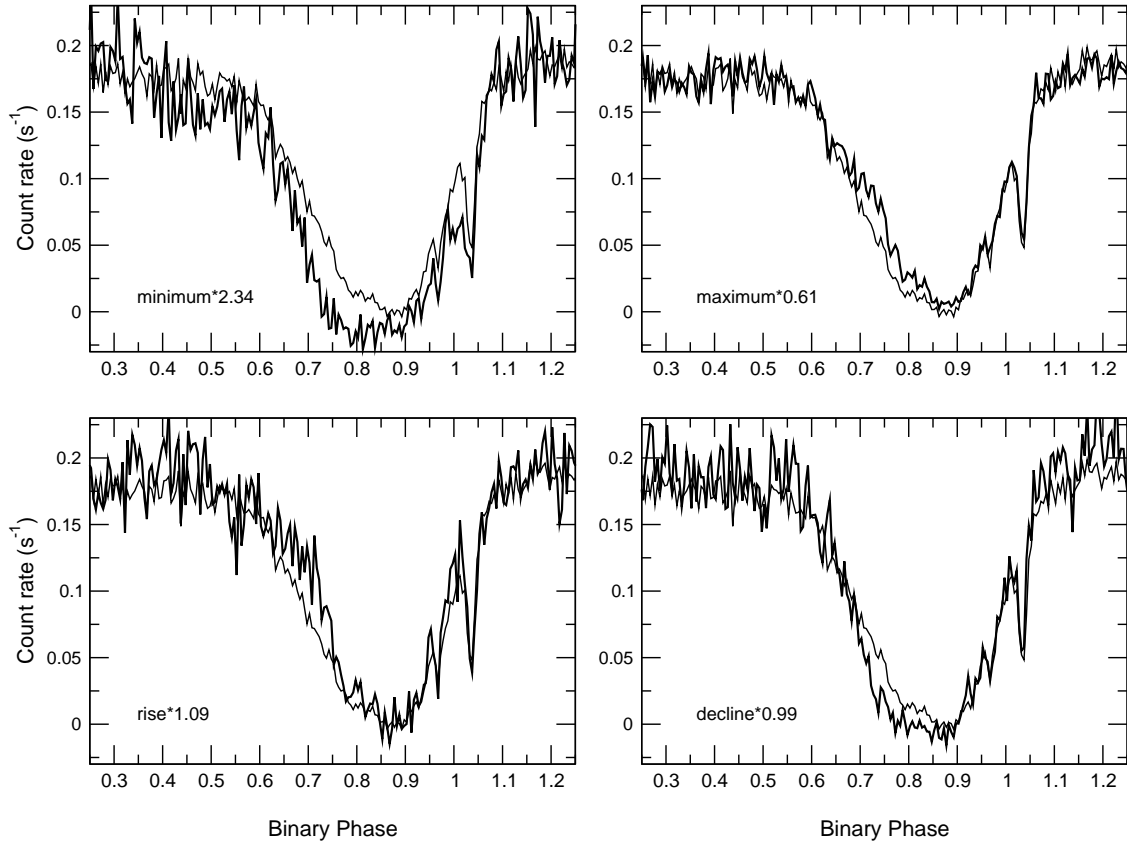


Fig. 4.— Plotted here are the data sets from the four spin phases, phased over the binary orbital period. Top left to right: spin minimum and spin maximum; bottom left to right: spin rise and spin decline. In each graph, the thick line represents the individual spin phase which has been scaled, for comparative purposes, to the mean level of the summed light curve (thin line) by the number indicated.



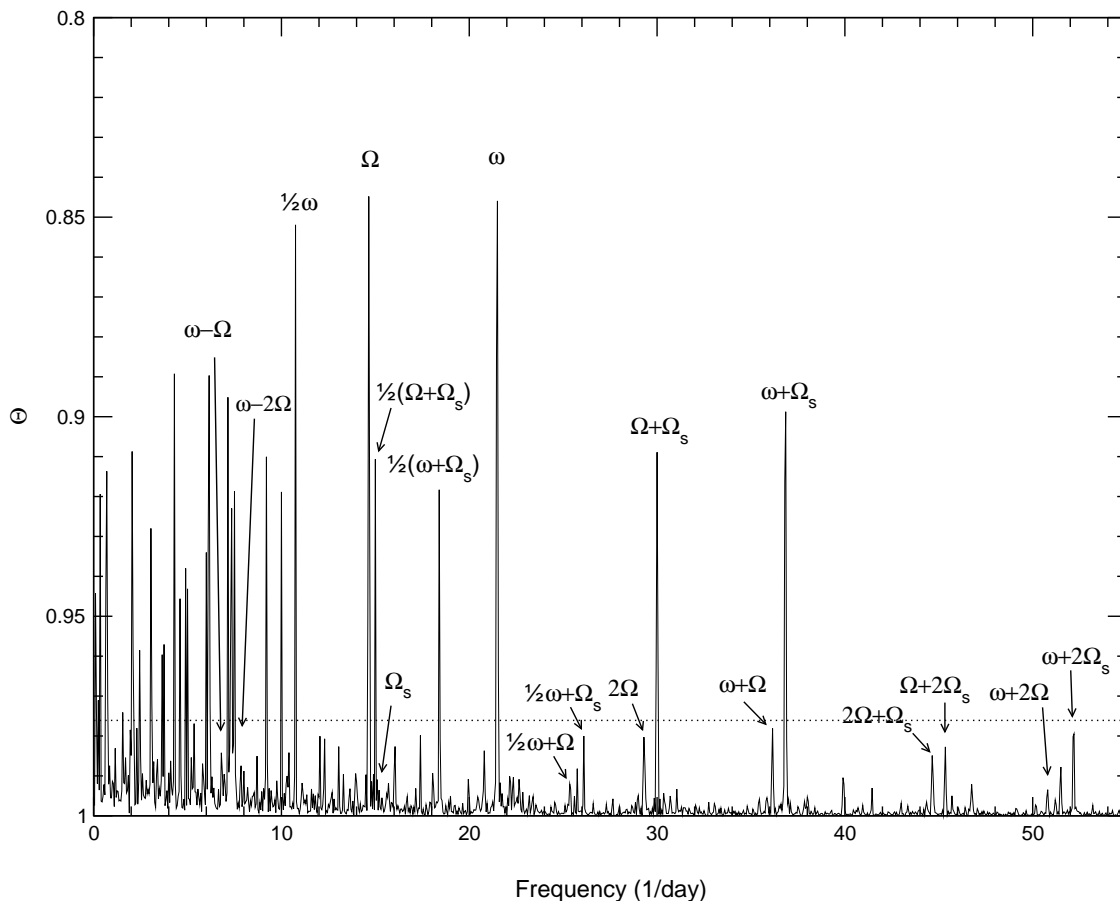


Fig. 5.— Thetagram of the EUV photometric data set. The known optical orbital sidebands are noticeable and have been labeled, where  $\omega$  represents the spin frequency,  $\Omega$  represents the binary frequency, and  $\Omega_s$  is the satellite orbital frequency. We have also labeled several other strong frequencies which we discuss in the text. The dashed line represents the 99% confidence level at 0.976 in power and the 95% confidence level is near 0.99 in power. The frequency resolution is 0.05.

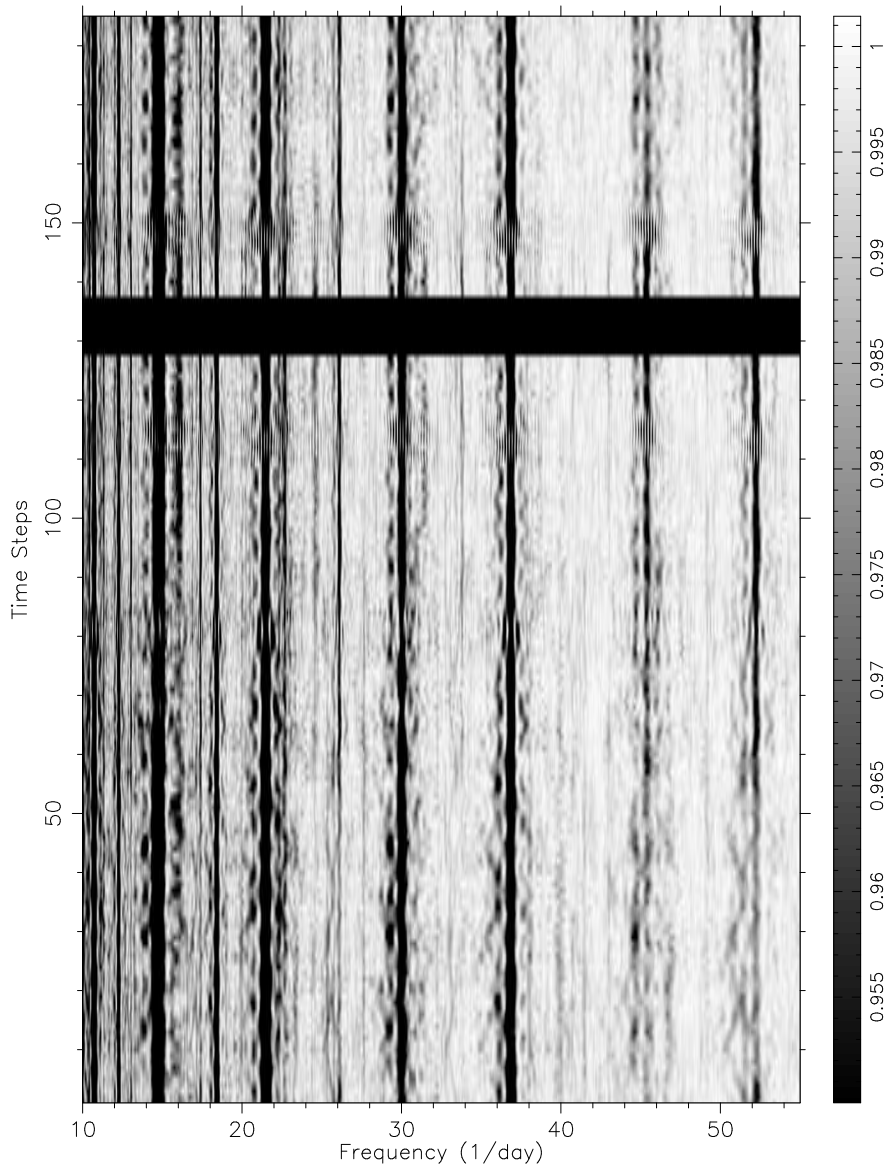


Fig. 6.— A time series thetogram of the EUV photometric data. The x-axis covers the frequency range  $10 - 55 \text{ day}^{-1}$  while the y-axis is time from the beginning to end of the *EUVE* observation. The gray scale indicates power, with darker areas corresponding to higher confidence levels; the color bar has the same numeric meaning as the y-scale in Figure 5. The more powerful frequencies seen in Figure 5 are also apparent here, and appear to remain constant throughout the time series, while less powerful frequencies come and go (e.g., see near  $25$  and  $33 \text{ day}^{-1}$ ). The region of missing data is due to a number of days with poor temporal sampling caused by an increased background level in the detector.

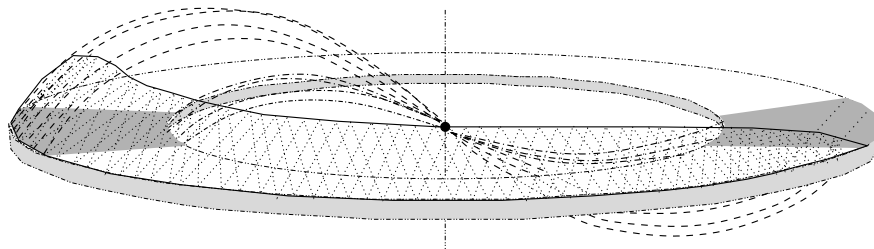


Fig. 7.— A schematic view of the inner accretion region in EX Hya. The parts of the accretion disk which may be corotating with the field lines are indicated (dark gray regions) and the extended bulge has been drawn (hatched region extending along the outer edge of the disk). The size of these regions are estimated. The dashed lines extending from the white dwarf to the inner and outer edges of the accretion disk represent the inner and outer accretion curtains, respectively. The view of EX Hya drawn here corresponds to binary phase  $\phi_{98} = 0.75$  and spin phase  $\phi_{67} = 0.75$ . The bulge would also extend below the orbital plane.